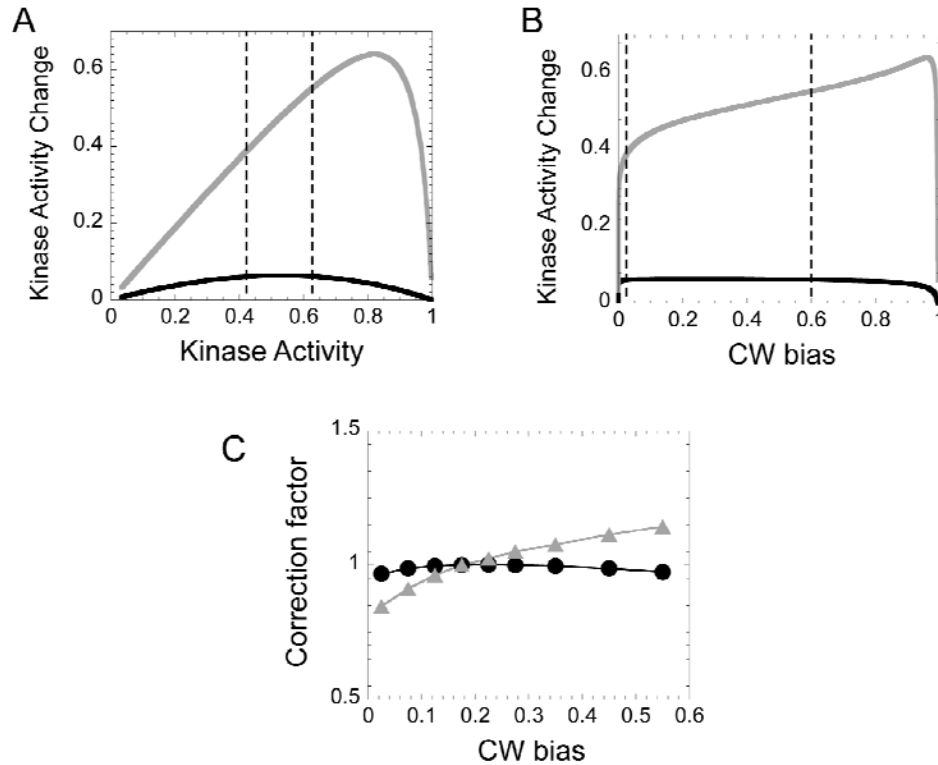


Supplementary Figure 1. CCW intervals after stimulus vs. CW bias before stimulus.

(a, c, and d) Individual cell measurements of the first, second, and third post-stimulus CCW intervals lengths vs. pre-stimulus CW bias for all cells (wild-type RP437 and RP437 expressing CheR from pZE21-CheR). Black (RP437 cells) and blue (RP437 cells expressing extra CheR from pZE21-CheR) circles, small stimulus (10 nM stepwise increase of L-aspartate). Grey (RP437 cells) and red (RP437 cells expressing extra CheR from pZE21-CheR) triangles, large stimulus (1 μ M stepwise increase of L-aspartate). Black line, the geometric means of the pre-stimulus CCW interval lengths for wild-type (RP437 and RP437 with extra CheR proteins expressed from a plasmid pZE21-CheR) cells as a function of the pre-stimulus CW bias as in (b).

(b) Mean pre-stimulus CCW interval length vs. pre-stimulus CW bias (\bar{b}). Black circles, wild-type RP437 cells. Grey circles, wild-type RP437 cells expressing extra CheR from pZE21-CheR. We used the geometric mean of the CCW interval lengths in each cell with a certain pre-stimulus CW bias. Black line, the power-law fit of the geometric mean of the CCW intervals before stimulus for all wild-type (with and without plasmid) cells as a function of the CW bias before stimulus ($\langle T^{CCW}(\bar{b}) \rangle_{before} \approx 0.29 \cdot \bar{b}^{-0.69} \text{ sec}$, $R^2=0.85$).

(e) Average length of the third post-stimulus CCW interval vs. pre-stimulus CW bias for all cells (wild-type RP437 and RP437 expressing CheR from pZE21-CheR). Black circles, CCW interval lengths after a small stimulus, grey triangles, CCW interval lengths after a large stimulus. Dark grey dotted line, geometric mean of the CCW interval lengths following a randomly chosen time point in non-stimulated cells. We used the geometric mean of the CCW interval lengths for each CW bias bin to remove the unusually dominant contribution to the mean due to the rare, extremely long CCW intervals. Black line, the power-law fit of the geometric mean of the pre-stimulus CCW interval length as a function of the pre-stimulus CW bias. Error bars show the standard errors for the average CCW interval length in each bin.



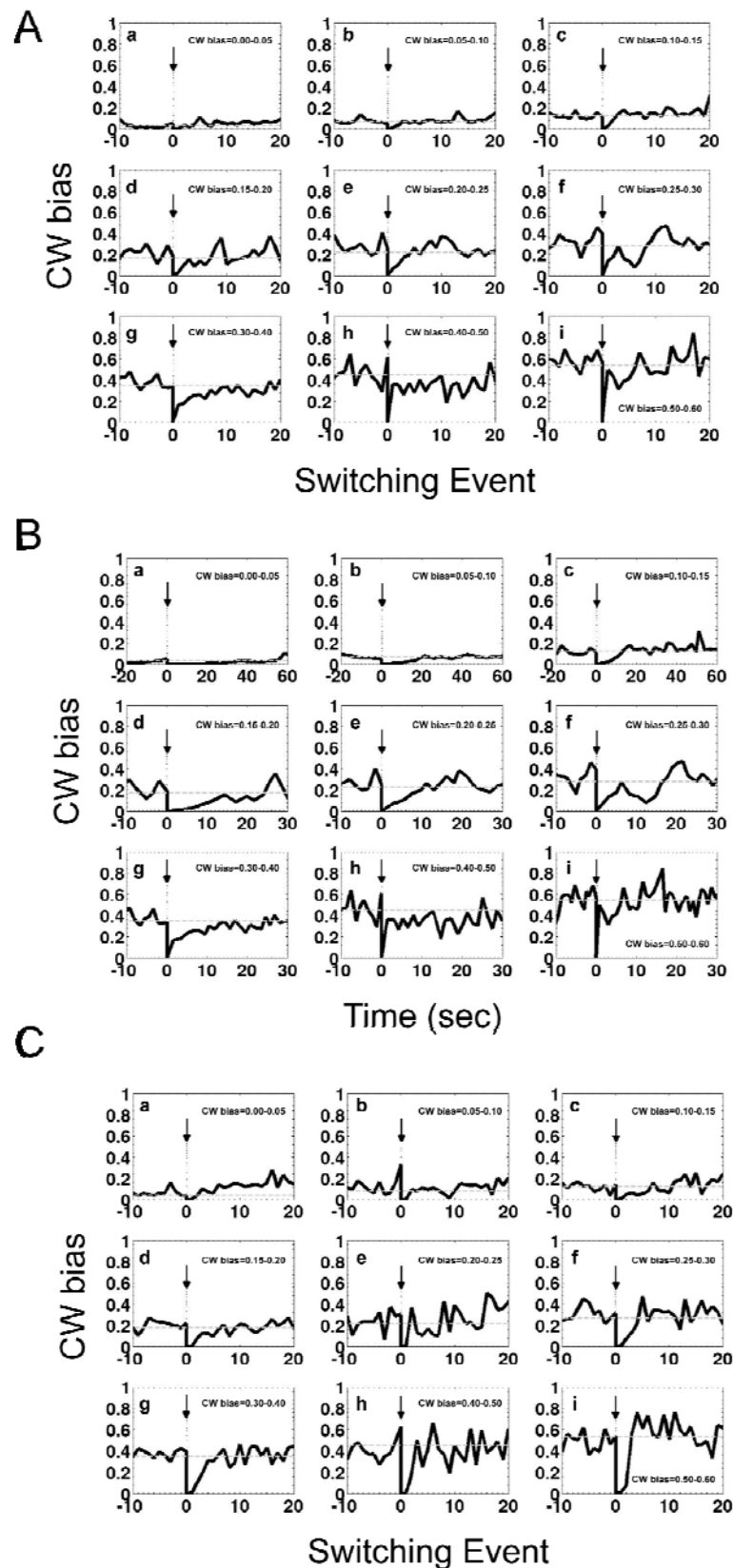
Supplementary Figure 2. Change in kinase activity over a range of CW biases.

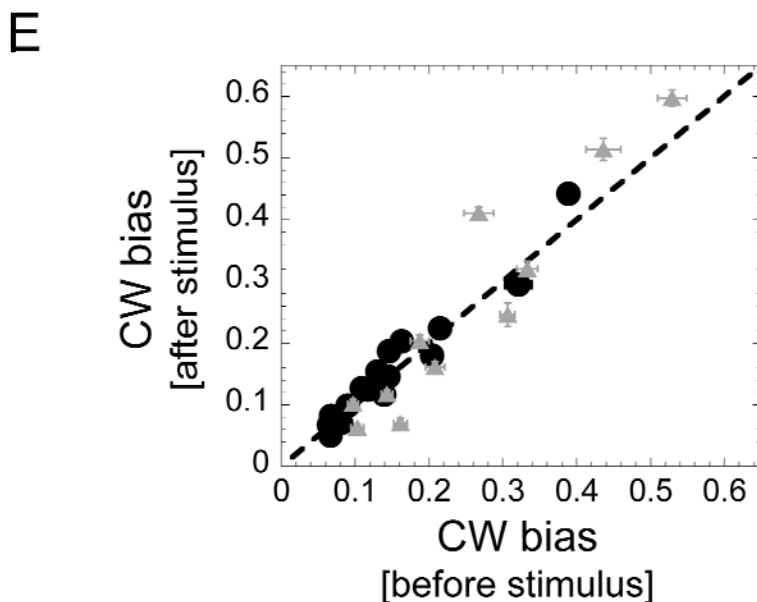
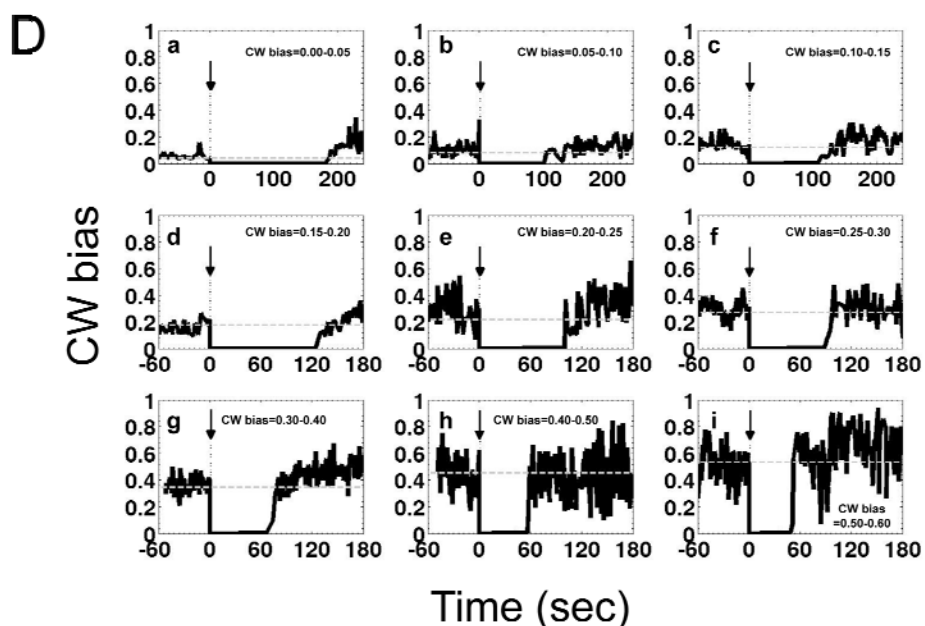
The underlying assumption of our experimental approach is that a specific stimulus causes an identical change in kinase activity for any functioning states of the cell. We will see that this assumption is correct for small stimulus whereas it needs to be corrected for large stimulus. To estimate the kinase activity change, we use a Monod-Wyman-Changeux model for a mixed cluster of 12 Tar and 24 Tsr receptors (*I-2*) with MeAsp as the external stimulus. The steady state of kinase activity at a total methylation level M (0 to 144) with a MeAsp concentration $[L]$ is given by

$$A^*(M, [L]) = \left[1 + e^{e_0 + e_1 \cdot M} \cdot \left(\frac{1 + \frac{[L]}{K_{Tar}^{off}}}{1 + \frac{[L]}{K_{Tar}^{on}}} \right)^{n_{Tar}/2} \cdot \left(\frac{1 + \frac{[L]}{K_{Tsr}^{off}}}{1 + \frac{[L]}{K_{Tsr}^{on}}} \right)^{n_{Tsr}/2} \right]^{-1}, \text{ where}$$

K_{Tar}^{off} , K_{Tar}^{on} , K_{Tsr}^{off} , and K_{Tsr}^{on} are the binding constants in the off and on states for the Tar and Tsr receptors, respectively, and n_{Tar} and n_{Tsr} are the number of Tar and Tsr receptors in the complex, respectively. Using dose-response data relating the change in kinase activity to MeAsp concentration (3), we fit the model parameters: $e_0 = 3.36$, $e_1 = -0.0632$, $K_{Tar}^{off} = 0.0094$ mM, $K_{Tar}^{on} = 0.0166$ mM, $K_{Tsr}^{off} = 150$ mM, $K_{Tsr}^{on} = 250$ mM. Based on kinase activity response to methyl-aspartate (MeAsp) (4) and L-Aspartate (5) in Tar⁺ cells, we determined that 1 μ M MeAsp corresponds to the small stimulus 10nM L-aspartate (black) and 100 μ M MeAsp corresponds to the large stimulus 1 μ M L-

aspartate (grey) used in our experiments. **(a)** Using this model, we determined the activity change, ΔA^* , due to the increase (ΔL) in MeAsp: $\Delta A^*([L] = 0 \mu\text{M}) - \Delta A^*([L] = 1 \mu\text{M})$ for small stimulus (black) or $\Delta A^*([L] = 0 \mu\text{M}) - \Delta A^*([L] = 100 \mu\text{M})$ for large stimulus (grey) as a function of the initial kinase activity before stimulus. **(b)** Kinase activity change as a function of the CW bias of an individual motor for small (black) and large stimulus (grey). To obtain this plot, we assumed a simple relationship between [CheY-P] and kinase activity [CheY-P] = (5.14 μM) $\times A^*$, ignoring the detailed kinetics of CheY phosphorylation. With the proportionality constant set to 5.14 μM , the average CW bias (~ 0.13) of wild-type cells corresponds to $A^* \sim 0.50$. We converted [CheY-P] to CW bias using a sigmoidal function fit to the data given in ref (6). The dotted lines bound the average methylation level and kinase activity to wild-type functioning range of the motor observed in our experiments: CW bias of 0.025 to and 0.600. Although the linear-response kinase activity change is $\sim A(1-A)$, in the regime studied in the experiments ($A = 0.4 - 0.6$), $A(1-A)$ is almost constant. **(c)** Based on the activity change in panel (b), we calculated a correction factor to estimate the response time of the kinase activity. Each point is the correction factor for a given CW bias bin relative to the peak at CW bias 0.15-0.20. The measured response time (T_A) of the kinase activity due to an external stimulus is related to the relaxation time τ_A as $T_A = \tau_A \cdot \ln \Delta A^*(t = 0; \Delta L) / \Delta A^*_{un}$, where ΔA^*_{un} is the undetectable level of the kinase activity from the steady state. The correction factor is the proportionality term between those two time scales, i.e. $\ln \Delta A^*(t = 0; \Delta L) / \Delta A^*_{un}$. We let $\ln \Delta A^*(t = 0; \Delta L) / \Delta A^*_{un} = 1$ for the wild-type state (CW bias=0.15-0.20). Black: 1 μM MeAsp, corresponding to 10 nM L-aspartate. Grey: 100 μM MeAsp, corresponding to 1 μM L-aspartate.

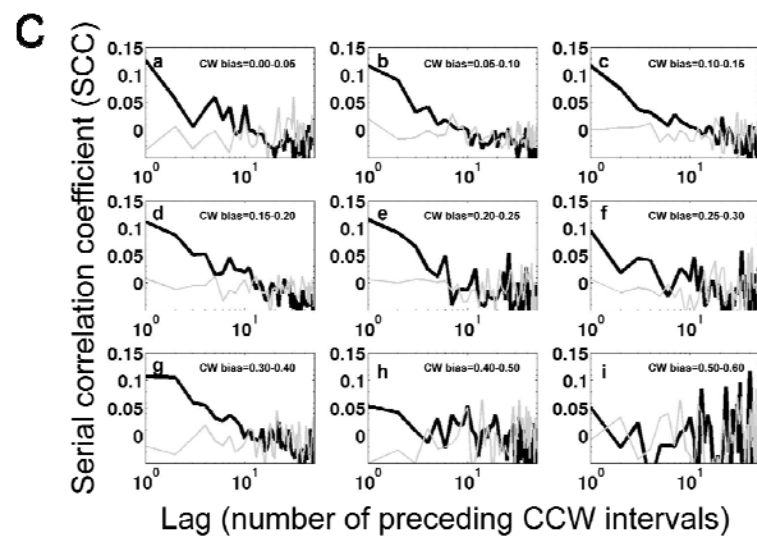
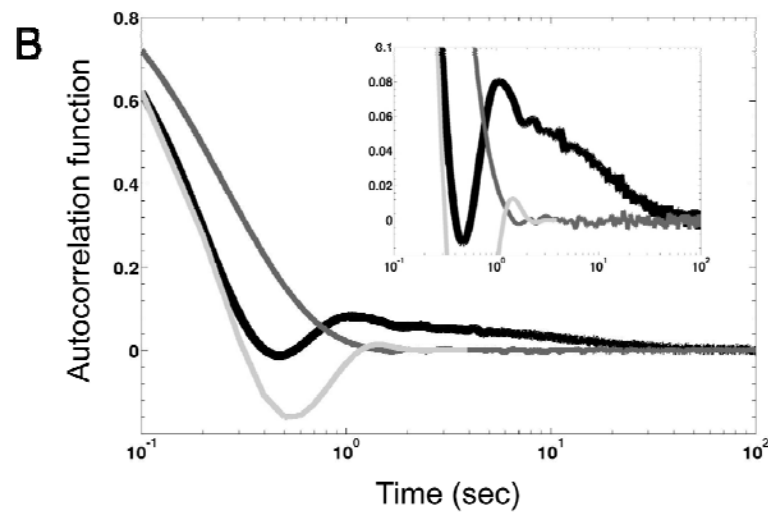
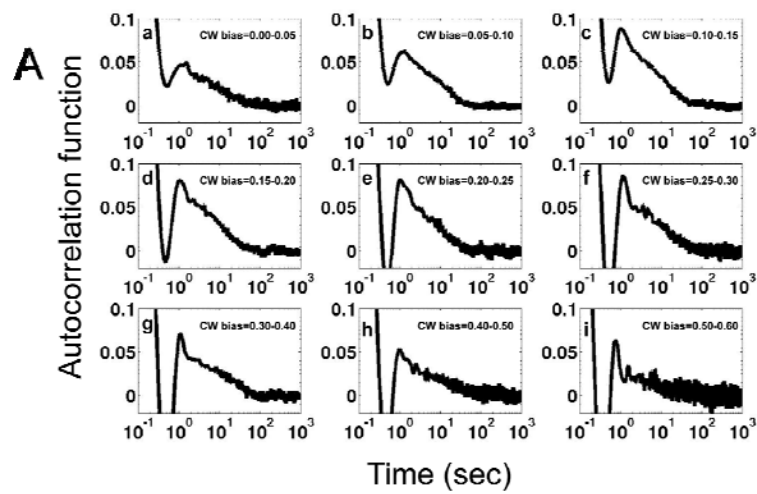


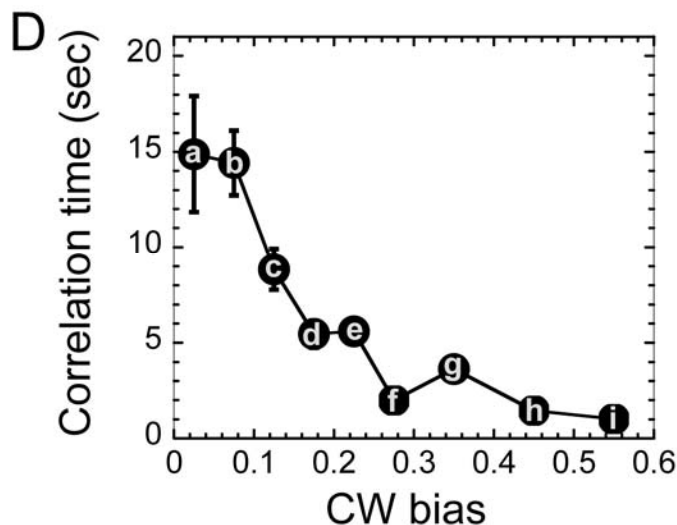


Supplementary Figure 3. Response and adaptation in chemotaxis at the single cell level.

(a and c) The short term CW bias as a function of the switching event after the stimulus (a: small stimulus; c: large stimulus). **(b and d)** The short term CW bias as a function of the time after the stimulus (b: small stimulus; d: large stimulus). Individual cells responded to a stepwise stimulus (increase) of L-aspartate (a and b: 10 nM; c and d: 1 μ M) released from caged L-aspartate at the zeroth switching event (black arrows). We recorded the binary time series of switching events between CW and CCW rotations of

one flagellum from each cell. The CW bias was averaged over all cells (wild-type RP437 and RP437 expressing CheR from pZE21-CheR) within the same CW bias bin. For b and d, we converted the switching events after the stimulus to the time duration using the geometric mean of CCW and CW interval lengths over all cells in each CW bias bin. (e) Adaptation in single wild-type cells (RP437 cells and RP437 cells expressing CheR) as a function of CW bias. The CW bias in single cells before stimulus is plotted against the CW bias after a small (black circles: 10 nM) or a large (grey triangles: 1 μ M) stepwise stimulus of L-aspartate. Black dotted line, near-precise adaptation for which the CW bias after stimulus equals the CW bias before stimulus. Error bars are the standard error.





Supplementary Figure 4. Correlation time

(a) Autocorrelation functions the 1500-second binary time series minus the average the CW bias in individual cells. We averaged the autocorrelation function over all cells (wild-type RP437 and RP437 expressing CheR from pZE21-CheR) with the same CW bias. We used the MatLab “xcorr” function to calculate the autocorrelation functions. (b) Black line: Average autocorrelation function of the wild-type (RP437 and RP437 with extra CheR expressed from pZE21-CheR) cells with CW bias=0.15-0.20. Dark grey line: Average autocorrelation function of fifty 1500-second binary time series simulated from a Poisson process with the average wild-type CW bias and with the typical switching rates of the motor. Light grey line: Theoretical calculation of the autocorrelation function for the binary time series composed of Gamma-distributed intervals with a CW bias ~0.2 from ref (7). The Gamma distributions for the CCW and CW durations of the motor are

$$G_r(t) = \frac{\nu^r t^{r-1} \exp(-\nu t)}{\Gamma(r)}$$

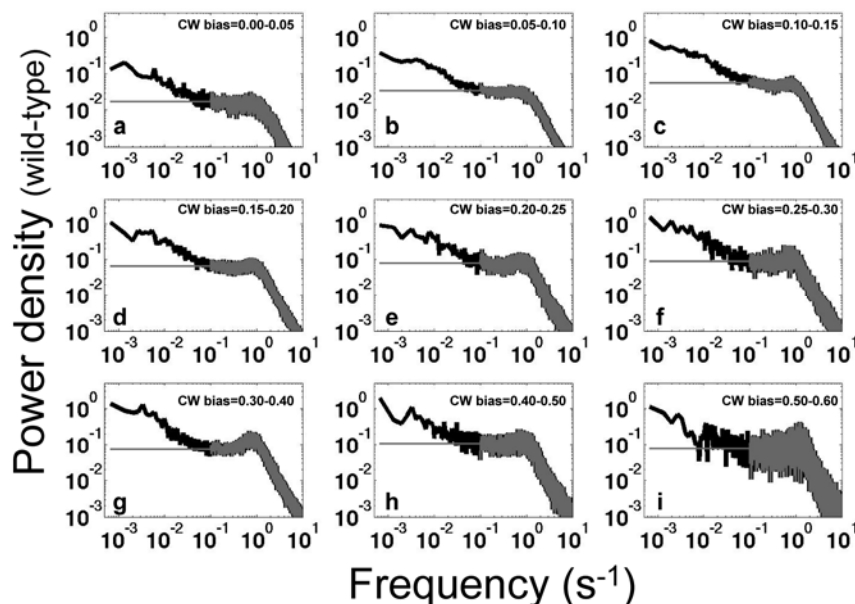
given by $\Gamma(r)$, where r and ν indicate the number of Poisson steps preceding a switch and the rate of underlying Poisson process, respectively. For the CW bias ~0.2, these two parameters have values $r = 3$ and $\nu = 2.5 \text{ s}^{-1}$ for CCW distributions and $r = 5$ and $\nu = 14.8 \text{ s}^{-1}$ for CW distributions (7). Inset, the magnified scale of the autocorrelation function from -0.02 to 0.1.

(c) Serial correlation coefficients (SCC) as a function of lags. We obtained the serial correlation coefficients (SCC) of 100 serial CCW intervals ($T_{i,j}^{CCW}$ is the length of the j^{th} CCW interval in the i^{th} cell, $j=1,2,3,\dots,100$) in individual cells. The SCC ($\rho_{i,\text{lag}}^{SCC}$) of 100 serial CCW intervals in the i^{th} cell is calculated as

$$\rho_{i,lag}^{SCC} = \frac{\sum_{j=1}^{100-1} \left(T_{i,j}^{CCW} - \langle T_{i,j}^{CCW} \rangle_j \right) \left(T_{i,j+lag}^{CCW} - \langle T_{i,j}^{CCW} \rangle_j \right)}{\left[\sum_{j=1}^{100-1} \left(T_{i,j}^{CCW} - \langle T_{i,j}^{CCW} \rangle_j \right)^2 \sum_{j=1}^{100-1} \left(T_{i,j+lag}^{CCW} - \langle T_{i,j}^{CCW} \rangle_j \right)^2 \right]^{1/2}}, \text{ where}$$

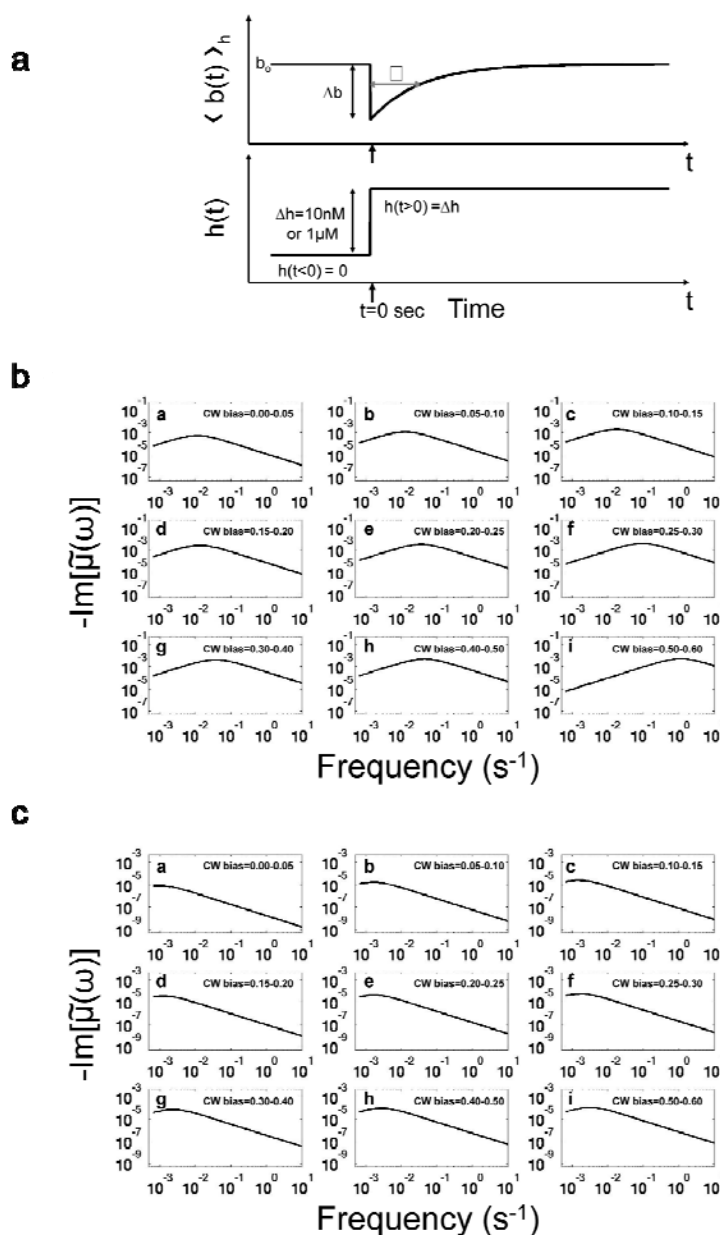
lag=0,1,2,... and $\langle T_{i,j}^{CCW} \rangle_j$ means the average length of the 100 CCW intervals in i^{th} cell.

We averaged the SCC values at each lag over all cells (wild-type RP437 and RP437 expressing CheR from pZE21-CheR) with the same CW bias (black lines). For each cell, we took a typical 100-interval series and reshuffled the series 300 times. We calculated the SCC of these 300 reshuffled series. We averaged the SCC values from the reshuffled series at each lag over all wild-type (RP437 and RP437 with extra CheR expressed from a plasmid pZE21-CheR) cells with the same CW bias (grey lines). **(d)** The average correlation time as a function of CW bias for wild-type (RP437 and RP437 expressing CheR from pZE21-CheR) cells. The letters correspond to the CW bias bins (Fig. 1a). The error bars are the average half-lengths of the first uncorrelated CCW intervals.



Supplementary Figure 5. Power spectral density averaged over the cells in the same CW bias bin.

The power spectral densities (black lines) averaged over all cells (wild-type RP437 and RP437 expressing CheR from pZE21-CheR) in the same CW bias bin. Power spectral density (dark grey lines) of the motor alone, which is decoupled from the signaling network. We approximated the baseline of the motor power density by finding the mean value of the flat regime (from $f_i = 1/10 s^{-1}$ to $f_f = 1/5 s^{-1}$) of the experimental power density and elongating the base line to the lowest frequency.



Supplementary Figure 6. Response functions of the output signals in Fourier space.

(a) Top, Schematic representation of the macroscopic average response $\langle b(t) \rangle_h$ with the steady-state $b_o = \langle b(t) \rangle_o$ before stimulus. In response to a stepwise stimulus $h(t) = \Delta h \cdot \Theta(t)$, where $\Theta(t)$ is a Heaviside step function, the average CW bias abruptly decreases by Δb , and then exponentially adapts back to the pre-stimulus steady state with the response time τ (grey arrow). To calculate the response function, we use the following model $\langle b(t) \rangle_h = b_o - \Delta b \cdot e(-t/\tau) \cdot \Theta(t)$ that reproduces accurately the known

macroscopic cellular response. **Bottom**, Schematic representation of a stepwise stimulus. In our experiments, the external stimulus function at time t is given by $h(t) = \Delta h = 10nM$ (small stimulus) or $h(t) = \Delta h = 1\mu M$ (large stimulus) for $t > 0$ s and $h(t) = 0nM$ for $t < 0$ s.

We calculated the response function $\mu(t)$, defined as $\langle b(t) \rangle_h - \langle b(t) \rangle_0 = \int_{-\infty}^t \mu(t-t')h(t')dt'$

in each CW bias bin, where the response time τ is obtained from Fig. 2a and the initial drop in CW bias Δb is given by Supplementary Fig. 2. Imaginary part of the Fourier transform of the response function for small (**b**) and large stimulus (**c**). We use

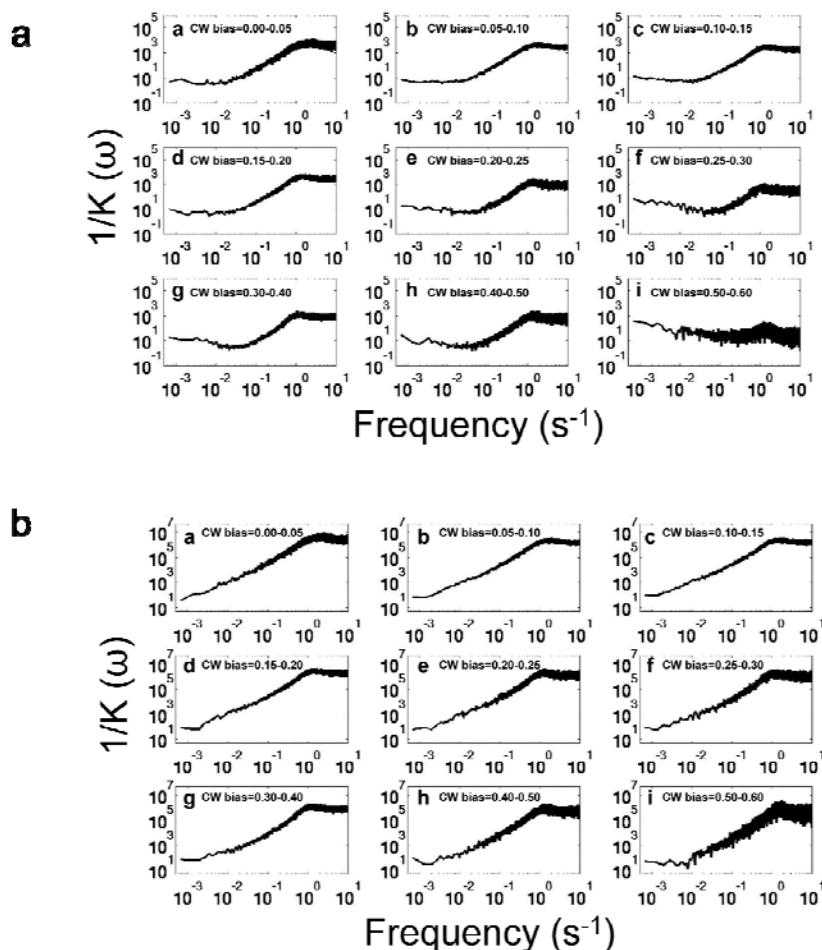
$\text{Im}[\tilde{\mu}(\omega)] = -\frac{\Delta b}{\sqrt{2\pi} \cdot \Delta h} \cdot \frac{\tau\omega}{1+(\tau\omega)^2}$, which is obtained from the Fourier transform of

$\langle b(t) \rangle_h - \langle b(t) \rangle_0 = \int_{-\infty}^t \mu(t-t')h(t')dt'$, where τ is the response time to the small or large

stimulus in each CW bias bin (Fig. 2a) and Δb is calculated using

$$\Delta b = b_o(\bar{Yp}) - b(\bar{Yp} - \Delta Yp) = \frac{\bar{Yp}^{N_H}}{K_M^{N_H} + \bar{Yp}^{N_H}} - \frac{(\bar{Yp} - \Delta Yp)^{N_H}}{K_M^{N_H} + (\bar{Yp} - \Delta Yp)^{N_H}}, \text{ where}$$

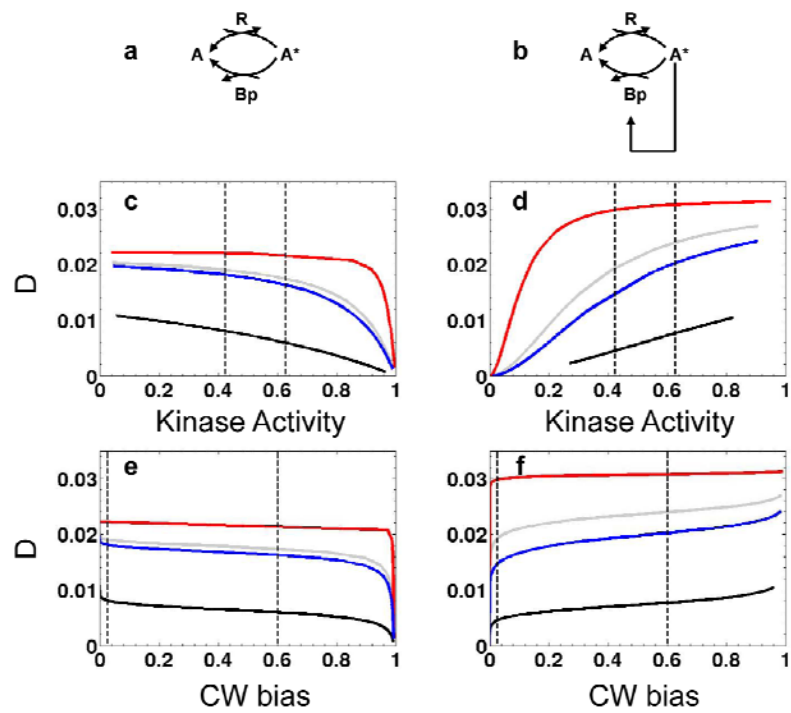
$\Delta Yp = 5.14\mu M \cdot \Delta A^*$ (Supplementary Fig. 2b).



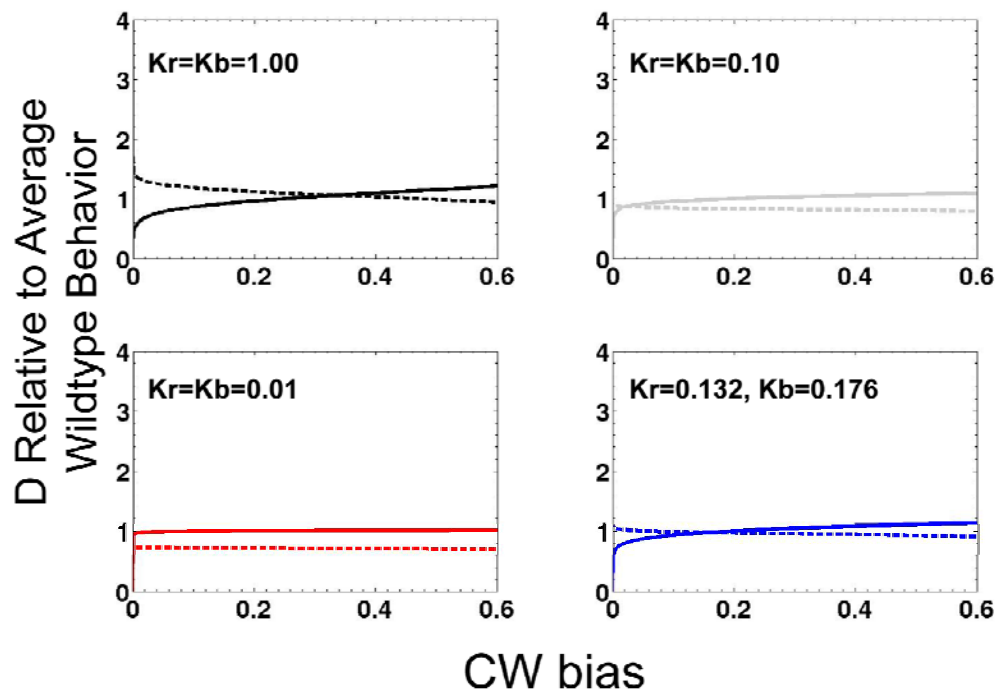
Supplementary Figure 7. Coupling coefficient $1/K(\omega)$, between spontaneous fluctuations and response function in Fourier space

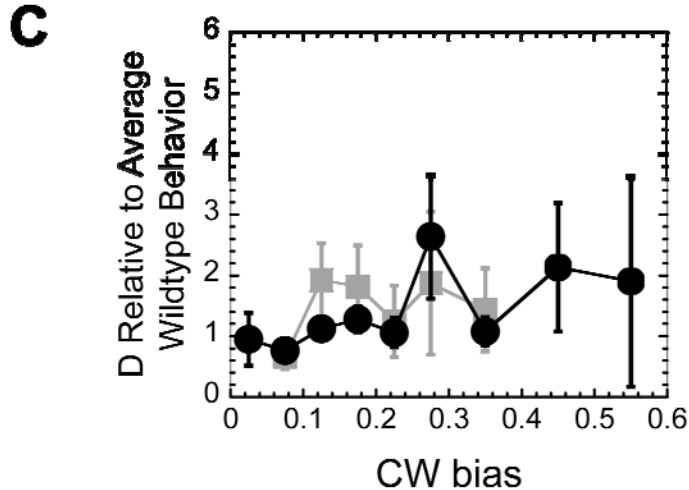
For (a) small and (b) large stimulus, the function $1/K(\omega) = -\omega P(\omega)/(2 \cdot \text{Im}[\tilde{\mu}(\omega)])$, where $P(\omega)$ is the average power spectral density in Supplementary Fig. 5 and $\text{Im}[\tilde{\mu}(\omega)]$ is the imaginary part of the Fourier transform of the response function due to a stepwise L-aspartate increase given in Supplementary Figs. 6b and c.

A



B





Supplementary Figure 8. Theoretical estimation of the Coefficient D using a simple kinetic model

The coefficient D is the strength of the spontaneous fluctuations taking place in a futile cycle associated with the methylation and demethylation reactions of receptors was

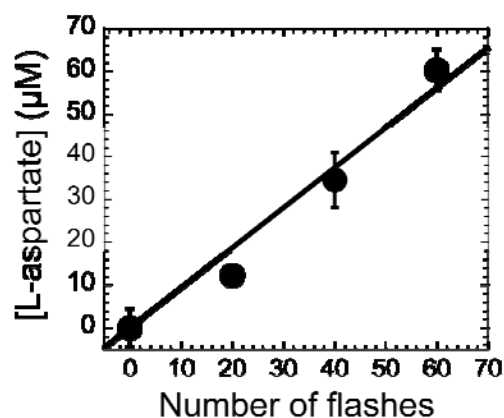
calculated using (8): $D \sim b \cdot A^* + r \cdot A$, where $b = \frac{k_b \varepsilon_{bp}}{K_b + A^*}$ and $r = \frac{k_r \varepsilon_r}{K_r + A}$,

where A^* is the concentration of free active kinase, ε_{bp} is the concentration of CheB-P, K_b is the Michaelis-Menten constant, k_b is the catalytic rate associated with demethylation and A is the concentration of free inactive kinase, ε_r is the concentration of CheR, K_r is the Michaelis-Menten constant, k_r is the catalytic rate associated with methylation. Importantly, the coefficient has strictly the same form as in ref. (9) where D was calculated for a vertebrate phototransduction cascade. **(a)** Using this simple assumption, we study the case without **(a-a)** and with **(a-b)** the CheB-P feedback loop (8) and found that the coefficient D is nearly constant in both cases. We confirmed this prediction with experimental data (see c) and compared D from wild-type cells with that of Δ CheB mutant cells missing the negative feedback loop. We calculated D values as a function of the total kinase activity without the CheB-P feedback loop **(a-c)** and with the CheB-P feedback loop **(a-d)**. Similarly, we plotted D as a function of the CW bias without the CheB-P feedback loop **(a-e)** and with the CheB-P feedback loop **(a-f)**. In all panels, we used four combinations of Michaelis-Menten constants (black: $K_r = K_b = 1.0$; grey: $K_r = K_b = 0.1$; red: $K_r = K_b = 0.01$; and blue: $K_r = 0.13, K_b = 0.18$, the wild-type values (8)). We can see that for all combination of Michaelis-Mentens constants the coefficient D is nearly constant within the functioning range of the motor. For the model without the CheB-P feedback loop we varied [CheB-P] and fixed [CheR] at the wildtype level. For the model with the CheB-P feedback loop, we varied [CheR]. The dotted lines show the kinase activity values corresponding to CW biases between 0.025 and 0.600, which represents the functioning range of the motor for wildtype cells. **(b)** Coefficient D

relative to that of wildtype cells as a function of CW bias. D was calculated for the models without the CheB-P feedback loop (dotted lines) and with the CheB-P feedback loop (solid lines) using the four combinations of the Michaelis-Menten constants from (A). The D values are normalized by the average D value over the CW bias range (0.025–0.600) in the model with the CheB-P feedback loop. These plots predict that the behavior of the coefficient D is robust to the deletion of the negative feedback loop in CheBp and is also insensitive to large variations of Michaelis-Menten constants. (C) Experimental data shows that the deletion of the negative feedback loop in the Δ CheB mutant cells (RP4972 and RP4992, gifts from J.S. Parkinson) does not affect the behavior of D . This plot shows D relative to that of wildtype cells as a function of CW bias for the

experimental data. The experimental D is defined as $D = 2 \cdot \frac{\sigma_{CheYp}^2}{\tau_{CheYp}}$. We estimated each

D value for wild-type cells (black circles: RP437 and RP437 expressing extra CheR from pZE21-CheR) and Δ CheB mutant cells without the CheB-P feedback loop (grey squares: RP4972 expressing CheBc from Lac-inducible plasmid pME304 (ref. (10)) and RP4992 expressing CheBc from LacR-inducible plasmid pZA32-CheBc and TetR-inducible plasmid pZA21-CheBc) in each CW bias bin. We normalized the D values in each CW bias bin by the mean value of D for wild-type cells. Error bars are the standard error. To construct pZA32-CheBc, we amplified the *cheBc* gene fragment from the chromosome of *E. coli* RP437 cells with primers CheBc-5': *gcg gta ccg cat gct gaa ggc ggg gcc gtt gtt g* and XbaI-CheB-3': *gct cta gat taa ata cgt atc gcc tgt c*. The gene fragment was inserted into the KpnI and XbaI sites of a pZA32 series plasmid that contained a chloramphenicol resistant cassette and a LacR inducible promoter. To construct pZA21-CheBc, we amplified the *cheBc* gene fragment from the chromosome of *E. coli* RP437 cells using the primers CheBc-5' and XbaI-CheB-3'. We inserted the gene fragment into the KpnI and XbaI sites of a pZA21 series plasmid that contained a kanamycin resistant cassette and a TetR inducible promoter.



Supplementary Figure 9. HPLC calibration of the released L-aspartate concentration from the caged L-aspartate solution as a function of the number of UV flashes.

The concentration of released L-aspartate fits linearly (solid line) with the number of UV flashes. Each 10 μL sample of 0.5 mM caged L-aspartate solution released about 1 μM L-aspartate per UV flash. Each data point is the average of 3 or 4 independent trials. Error bars show the standard deviation.

References

1. J. E. Keymer, R. G. Endres, M. Skoge, Y. Meir, N. S. Wingreen, *Proceedings of the National Academy of Sciences of the United States of America* **103**, 1786 (Feb 7, 2006).
2. B. A. Mello, Y. H. Tu, *P Natl Acad Sci USA* **102**, 17354 (Nov 29, 2005).
3. V. Sourjik, H. C. Berg, *Proc Natl Acad Sci U S A* **99**, 123 (Jan 8, 2002).
4. V. Sourjik, H. C. Berg, *Nature* **428**, 437 (Mar 25, 2004).
5. A. Vaknin, H. C. Berg, *Journal of Molecular Biology* **366**, 1416 (Mar 9, 2007).
6. P. Cluzel, M. Surette, S. Leibler, *Science* **287**, 1652 (Mar 3, 2000).
7. E. A. Korobkova, T. Emonet, H. Park, P. Cluzel, *Phys Rev Lett* **96**, 058105 (Feb 10, 2006).
8. T. Emonet, P. Cluzel, *Proc Natl Acad Sci U S A* **105**, 3304 (Mar 4, 2008).
9. P. B. Detwiler, S. Ramanathan, A. Sengupta, B. I. Shraiman, *Biophys J* **79**, 2801 (Dec, 2000).
10. W. E. Balch, *J Biol Chem* **264**, 16965 (Oct 15, 1989).